

## FOCUS REVIEW

## Strength and toughness of bio-fusion materials

Ko Okumura

In nature, there are many strong and tough biomaterials that result from the fusion of soft and hard elements. These materials include nacre, crustacean exoskeletons and spider webs. Here, we review previous studies on such bio-fusion materials, emphasizing the importance of simple models to gain a physical understanding of the emergence of strength and toughness from these structures. Thus, a simple understanding obtained through biologically inspired models provides useful guiding principles for the development of artificial tough composites by mimicking biomaterials.

*Polymer Journal* (2015) 47, 99–105; doi:10.1038/pj.2014.97; published online 5 November 2014

## INTRODUCTION

Various animals and plants in nature have developed strong and tough materials, often with magnificent hierarchical structures.<sup>1–4</sup> Nacre, a glittering layer found on the surface of pearls or inside certain seashells, is one such example: hard layers are glued together by thin soft adhesive sheets,<sup>5</sup> which results in remarkable strength and toughness.<sup>6</sup> In the exoskeleton of crustaceans, helically oriented soft fibers are embedded in a hard matrix, which achieves excellent mechanical performance.<sup>7</sup> There are many porous and strong materials in nature, such as the stereom in adult skeletal plates of echinoderms or holothurians,<sup>8</sup> the skeleton of a particular sponge,<sup>9</sup> and the frustules of diatoms.<sup>10</sup>

In these examples, a common strategy is the fusion of soft and hard elements (porous materials are considered an extreme case). Spider webs are such an example, with the web consisting of hard radial threads and soft spiral threads.

In this review, together with a discussion of references on each subject, we approach some of these examples of soft–hard fusion materials found in nature using simple models. As a result, we obtain scaling laws and gain a clear physical understanding of the mechanical advantages of the model composite structures. Such a simple understanding could be useful because they may provide guiding principles to develop artificially strong composite materials.

## NACRE

Nacre has been well-studied as a representative of tough and strong biomaterials exhibiting magnificent hierarchical structures,<sup>11–14</sup> together with, for example, bone,<sup>15–17</sup> and has led to a number of bioinspired materials.<sup>18–23</sup> In the layered structure of nacre, hard plates of aragonite are adhered together by thin and soft layers of proteins between the thick and hard plates:<sup>11</sup> the fracture surface energy of nacre was shown to be a few thousand times as high as that

of a monolith of the hard element.<sup>6</sup> In recent years, more detailed substructures have been found.<sup>24–26</sup>

There has been a controversy regarding the elastic behavior of nacre's soft element. The estimation of the modulus ranges from 4 GPa<sup>6</sup> to 100 Pa.<sup>27</sup> However, the soft protein-based elements have been observed to behave like gels.<sup>5</sup> A typical value of the elastic modulus of such gels could be approximately 1 MPa,<sup>28</sup> which is consistent with the recent observation in Barthelat *et al.*<sup>26</sup>

Various mechanisms for nacre's toughness and strength have been proposed on the basis of experimental observations, such as stepwise elongation,<sup>29</sup> thin compressive layers,<sup>30</sup> rough layer interfaces,<sup>31</sup> mineral bridges<sup>32</sup> and wavy surfaces of the plates.<sup>26</sup>

Various theoretical considerations have also been made, which include (1) elastic models<sup>30</sup> based on analytical solutions<sup>28,33</sup> and scaling arguments,<sup>34,35</sup> (2) viscoelastic models,<sup>36</sup> (3) micromechanical models,<sup>37</sup> (4) several numerical models such as finite-element models,<sup>26,38,39</sup> a fuse network model<sup>40</sup> and a model with a periodic Young's modulus.<sup>41</sup>

Below, we focus on a simple model of nacre.<sup>28</sup> In the model, simple scaling laws were obtained to predict the correct order of the fracture energy of nacre based on analytical solutions.<sup>28,42</sup>

## Simple layered model of nacre

In the simplified view, the layered structure consists of thick and hard layers, as well as thin and soft layers, as indicated in Figure 1. The model is specified by the hard and soft linear elastic moduli ( $E_h$  and  $E_s$ ) and the thicknesses of soft and hard layers ( $d_h$  and  $d_s$ ) that satisfy  $E_h \gg E_s$ ,  $d_h \gg d_s$ . We consider cases in which a macroscopic line crack much larger than the layer period ( $d = d_h + d_s$ ) propagates perpendicular to the layers as in Figure 1 in the limit of small  $\varepsilon$ , where  $\varepsilon$  is defined by  $\varepsilon = d/d_s \cdot E_s/E_h \ll 1$ . This factor is indeed smaller than unity in the case of nacre. Typical values are as follows:

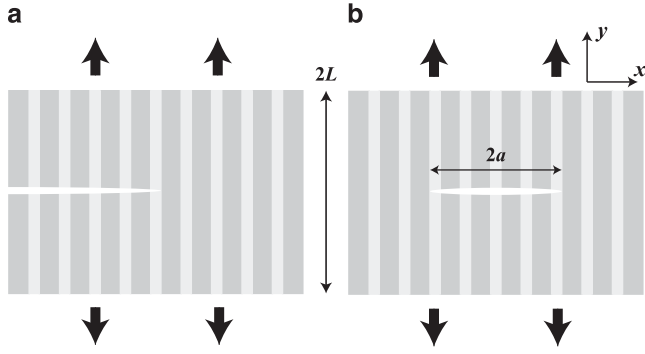


**Figure 1** Two boundary conditions solved analytically for a semi-infinite plate. (a) Semi-infinite plate of nacre with a semi-infinite crack propagating in the direction perpendicular to the layers. (b) Semi-infinite plate of nacre with a crack of the finite size  $2a$ . In both cases, the magnitude of the strain at the edges at  $y = \pm L$  is fixed as  $u_0$  (the upper and lower ends of the plates are subject to non uniform tensile stress, which is implied by the four thick arrows). The stress at the fracture surfaces is set to zero.

$d_h = 0.5 \mu\text{m}$ ,  $d_s/d_h$ ,  $E_h = 50 \text{ GPa}$  and  $E_s = 1 \text{ MPa}$  (the soft layers are like gels).<sup>5</sup> This set gives  $\varepsilon \sim 1/10\,000$ .

### Scaling laws for stress concentration and crack shape

The leading-order contribution in terms of  $\varepsilon$  of the anisotropic energy of the simple model of nacre results in an anisotropic Laplace equation. For the equation, two boundary problems, illustrated in Figures 1a and b, have been solved analytically in Okumura and de Gennes<sup>28</sup> and Hamamoto and Okumura,<sup>42</sup> respectively. The full analytical solutions simplify near a crack tip to give scaling laws. For the boundary condition illustrated in Figure 1a, the line crack is located at  $y=0$  and  $x < 0$  under no tensile stress. Under a finite stress the crack opens, for example, the upper crack surface is obtained as a deformation field at  $y=0^+$  and  $x < 0$ , where  $y=0^+$  denotes the limit approaching  $y=0$  from above. Similarly, the stress field at  $y=0$  is branched into two solutions (the stress for  $x > 0$  is positive and that for  $x > 0$  is negative). Under the boundary condition in Figure 1a, the deformation and stress (the  $yy$  component) at  $y=0^+$  near a crack tip at the distance  $r$  from the tip are given by

$$u(r) \simeq u_0 \sqrt{(r/\sqrt{\varepsilon})/L} \quad (1)$$

$$\sigma(r) \simeq \sigma_0 \sqrt{L/(r/\sqrt{\varepsilon})} \quad (2)$$

where  $u_0$  is the magnitude of remote stress at the edges and  $\sigma_0$  is defined as  $\sigma_0 \simeq \varepsilon u_0/L$ . Here, the notation  $X \simeq Y$  suggests that  $X$  and  $Y$  are equal at the level of scaling laws, that is, equal except for a dimensionless numerical coefficient. The above scaling laws are valid in the limit,

$$d_s \ll d_h < d \ll r \ll \sqrt{\varepsilon}L \quad (3)$$

In Equations (1) and (2), the stress concentration is mitigated by the small factor  $\varepsilon^{1/4}$ , whereas the deformation near the tip is enlarged by the large factor  $\varepsilon^{-1/4}$ , compared with the non-layered case.

Hamamoto and Okumura<sup>42</sup> shows that Equations (1) and (2) are valid in a wide range. They are also correct for the boundary condition in Figure 1b in the ‘large’ crack limit  $a \gg \sqrt{\varepsilon}L$ ; when  $a \simeq L$  and even when  $a < L$ , only if  $a \gg \sqrt{\varepsilon}L$  for small  $\varepsilon$ , the ‘large’ crack limit is appropriate, which implies a wide applicability of this limit.

### Fracture strength and toughness of nacre

The failure stress of nacre (in the large crack limit) is obtained as

$$\sigma_f \simeq \varepsilon^{-1/4} \sqrt{d/a_0} \sigma_h \quad (4)$$

where  $\sigma_h$  is the failure stress for a monolith of the hard material, showing the large enhancement factor  $\varepsilon^{-1/4} \sqrt{d/a_0}$  for the strength ( $d \gg a_0$ ). This equation is derived by matching two stresses: (I) an intrinsic failure stress of the hard layer of thickness  $\simeq d$  without any macroscopic cracks but with small defects of size  $a_0$ , which act as small cracks of size  $a_0$ , and (II) the stress in Equation (2) estimated at  $r=d$ , below which the continuum description is no longer possible (the maximum stress that appears near the tip should be cutoff in a continuum model).

This matching condition also leads to the fracture surface energy of nacre:

$$G_c \simeq \varepsilon^{-1/2} (d/a_0) G_h. \quad (5)$$

where  $G_h$  is the toughness of the monolith. The large enhancement factor  $\varepsilon^{-1/2} (d/a_0)$  found here for the toughness is estimated to be approximately 1000 for the typical values quoted above and is comparable to the classic experimental result.<sup>6</sup>

### Guiding principles

From Equations (4) and (5), we observe some guiding principles for soft–hard layer composites. For example, when defect sizes in the hard layers are comparable to the thickness of the soft layers ( $a_0 \simeq d_s$ ), large values of the factors  $d_h/d_s$  and  $E_h/E_s$  are advantageous.

### Finite-element calculations

The above model of nacre was examined using a finite-element model.<sup>43</sup> As shown below, this finite-element study shows that the scaling predictions given above are robust.

In the finite-element calculations, we examined the above scaling laws in the ‘large’ crack limit, which requires the conditions

$$d_s \ll d_h < d \ll r \ll \sqrt{\varepsilon}L \ll a \ll L_x \quad (6)$$

The sample half-length in the  $x$  direction  $L_x$  is assumed infinite in the derivation of the analytical solutions; however, it is set to a finite value in the simulations.

This set of conditions is numerically demanding because there are many length scales that should be well separated. The parameters were set as follows:  $d_h = 10d_s$ , the full dimension of the sample  $2L = 2L_x = 10\,000d_s$ , the half-crack size  $a = 495d_s - 530d_s$ ,  $\varepsilon = \varepsilon_0 (= 1/6500)$ ,  $6.5\varepsilon_0 (= 1/1000)$ ,  $6.5\varepsilon_0 (= 1/100)$  and 1. The case  $\varepsilon = \varepsilon_0$  mimics nacre and  $\varepsilon = 1$  corresponds to a monolith of the hard element.

The above parameter settings satisfy only marginally or even slightly violate the set of conditions in Equation (6). The condition  $\sqrt{\varepsilon}L \ll a$  is violated for  $\varepsilon = 65\varepsilon_0$  because  $\sqrt{\varepsilon}L \simeq a$  in this case. The condition  $d \ll r \ll \sqrt{\varepsilon}L$  allows only a small range for  $r$  especially for  $\varepsilon = 65\varepsilon_0$ : the scaling predictions are guaranteed only in the region  $10d_s \ll r \ll 50d_s$  for  $\varepsilon = 65\varepsilon_0$ .

As shown in Figure 2, the stress concentration in nacre ( $\varepsilon = \varepsilon_0$ ) is significantly reduced compared with a monolith of the hard element ( $\varepsilon = 1$ ). In addition, the numerical results provide a simple physical understanding of the stress concentration reduction: the deformation in the hard layers, which governs the stress, is reduced in exchange for large deformation in the soft layers,<sup>44</sup> as demonstrated in Figures 3a and b (This mechanism is similar to that found in the shear-lag model).<sup>45</sup>

The predicted scaling laws are shown to be valid and robust through the expected collapse shown in Figures 3c and d. In addition, the

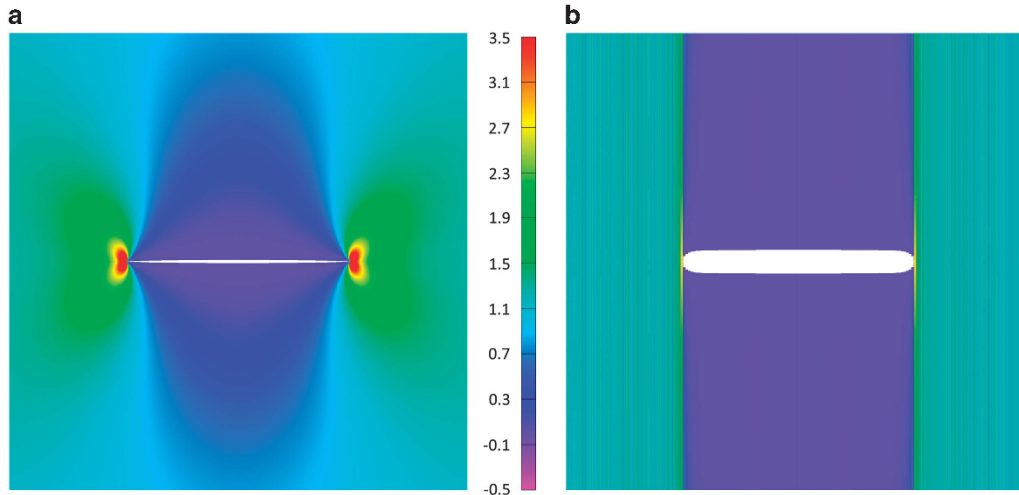


**Figure 2** Stress distribution in a sample with a line crack in the center, obtained by the finite-element calculation. (a) Monolith of the hard material contained in nacre. (b) Model of nacre consisting of layers of hard and soft materials. Stress concentration near the crack tips are significantly reduced in (b). Produced from the data in Hamamoto and Okumura.<sup>43</sup>

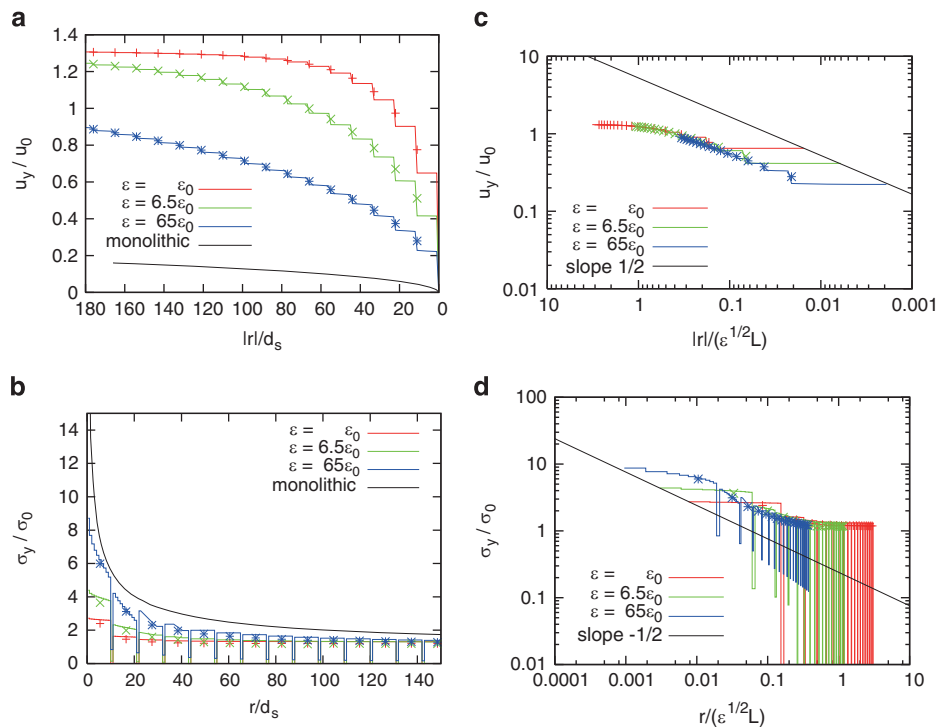


**Figure 3** Crack shape and stress distribution around the right tip of the horizontal line crack obtained from the finite-element calculation. (a) Crack shape near the right crack tip located at  $r=0$ . The deformation is more enhanced by soft layers as  $\epsilon$  decreases. (b) Stress distribution near the right crack tip located at  $r=0$ . The stress is more reduced as  $\epsilon$  decreases. (c) and (d) Collapse of the data in (a) and (b), respectively, by the scaling laws, as predicted by the theory. Reprinted from Hamamoto and Okumura<sup>43</sup> © 2009 WILEY-VCH Verlag GmbH & Co. KGaA, Weinheim.

assumption invoked above when deriving Equation (4), that is, the stress should be cutoff at a crack tip at approximately  $r=d$ , is also well confirmed in Figure 4a. Furthermore, a mechanism of crack arrest by the soft layers is demonstrated in Figure 4b; In Figure 4b, the tip stress increases as the tip propagates from a soft layer to hard layers and decreases when the tip arrives at the next soft layer, implying that crack tips tend to stop at a soft layer.

## EXOSKELETONS OF CRUSTACEANS

In the cuticle of the exoskeleton of lobsters, which is a tough and strong layer, bundles of chitin-protein fibers are embedded in a calcium carbonate matrix. The bundles are oriented parallel to each other at the surface of the cuticle, and the orientation rotates toward the inside. However, compared with the well-studied nacre, the hierarchical structure, which is universal in crustaceans,<sup>46</sup>

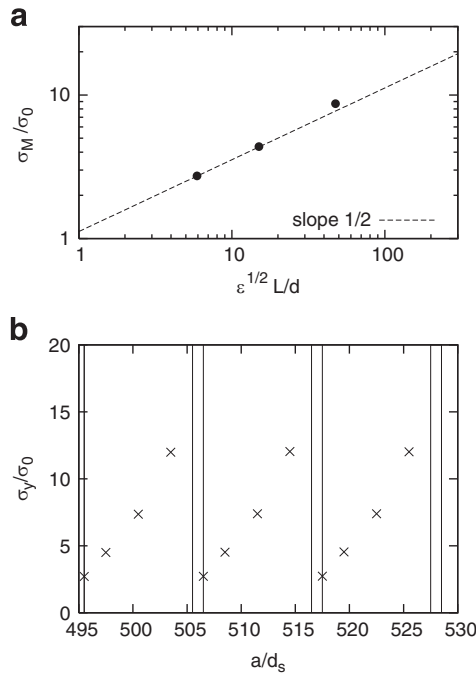


**Figure 4** Results from the finite-element calculation. (a) Confirmation of the scaling law for the maximum stress when crack tips are located at soft layers. (b) The crack tip stress, that is, the maximum stress, as a function of crack tip positions, showing the tendency for crack tips to stop at soft layers in which the tip stress is small. The vertical lines represent the boundary between soft and hard layers. Reprinted from Hamamoto and Okumura<sup>43</sup> © 2009 WILEY-VCH Verlag GmbH & Co. KGaA, Weinheim.

and its mechanical properties have been studied only recently.<sup>7,47</sup> Artificial biomineralization has been studied to mimic the structure.<sup>49–51</sup> Here, we review a simple model of the helical structure,<sup>52</sup> in which only the leading contribution is considered in the limit of a small parameter  $\epsilon'$ .

The exoskeleton of crustaceans is covered with three cuticle layers: the epicuticle, exocuticle and endocuticle layers, from the surface to the inside. The epicuticle is a waxy layer that lacks a special structure; however, the exo- and endocuticles possess a remarkable helical structure consisting of bundles and matrix, as already discussed.

The exo- and endocuticles can be regarded as a composite of soft and hard elements similar to nacre: the bundles are softer than the matrix. However, the elements are not simply layered but composed of bundles, embedded in a matrix, forming a helical structure. The helical pitch of the endocuticles is several times larger than that of the exocuticle. The volume percentage of the soft and hard elements are nearly the same, which is not the case for nacre.

Based on these features, we introduce the elastic modulus of the bundles  $E_b$  ( $\approx 1$  GPa) and of the matrix  $E_m$  ( $\approx 100$  GPa), together with the volume fractions of the bundle  $\phi_b = (1+\delta)/2$  and of the matrix  $\phi_m = (1-\delta)/2$ , and we require the following conditions:

$$E_b \ll E_m \text{ and } \delta \ll 1 \quad (7)$$

Considering the two modes of deformation illustrated in Figure 5, in addition to the aid of the standard arguments for fiber composites,<sup>53</sup> the corresponding hard and soft moduli ( $E'_h$  and  $E'_s$ ,

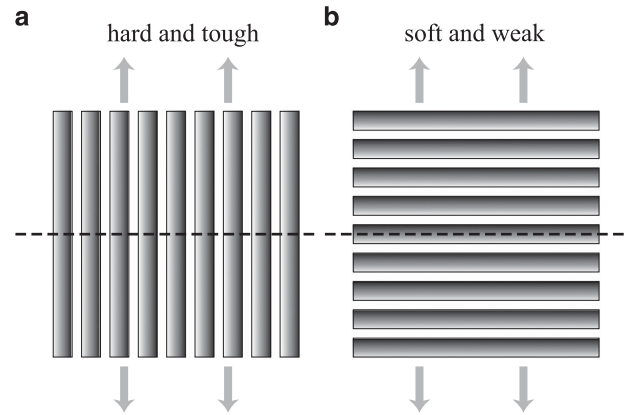


**Figure 5** Bundle embedded in a matrix (the matrix is not shown) in the 'parallel structure' under tensile force in longitudinal (a) and transverse (b) directions. When the composite is under tension as indicated by the arrows, the composite is hard and tough in the longitudinal direction and soft and weak in the transverse direction. The dashed line indicates a possible crack surface.

respectively) are evaluated as

$$E'_h \simeq \phi_b E_b + \phi_m E_m \quad (8)$$

$$1/E'_s \simeq \phi_b/E_b + \phi_m/E_m \quad (9)$$

We introduce a small parameter  $\epsilon'$  as

$$\epsilon' = E'_s/E'_h \ll 1. \quad (10)$$

The fracture toughness of the parallel structure should be direction dependent and those in the soft and hard directions shown in Figure 5 are introduced as  $G_h$  and  $G_s$ . They satisfy

$$G_h \gg G_s, \quad (11)$$

which should be intuitively natural for fiber bundles (see Okumura<sup>52</sup> for the detailed supporting discussions).

We next consider the helical structure in the exoskeleton. As the elastic modulus periodically changes along the axis of the helical structure,<sup>41,54–57</sup> we consider, at a coarse-grained level, a layered structure in which the elastic moduli of the hard and soft layers are characterized by  $E'_h$  and  $E'_s$  and the helical pitch  $d$  corresponds to the thickness of both of the layers.

Through this two-step coarse-graining process, we can now estimate the fracture toughness by applying the results obtained for the simple model of nacre. This estimation is possible because the nacre theory is developed in the limit  $\epsilon = (E_s/E_h)(d_h/d_s) \ll 1$ , which is also satisfied in the present case in which  $E_s = E'_s \gg E_h = E'_h$ , that is,  $\epsilon' \ll 1$ , and  $d_h = d_s = d$ .

From Equation (5), the fracture toughness of the helical structure, when a line crack of size  $a$  that is larger than  $d$  is running perpendicular to the layers, is thus obtained as

$$G/G_h \simeq (d/a_0)(\epsilon')^{-1/2} \quad (12)$$

with

$$(\epsilon')^{-1} \simeq (1+\delta)(1-\delta)E_m/E_b \quad (13)$$

Here  $a_0$  is the size of the Griffith flaws in the hard layer, which may be comparable to the radius of the bundles ( $\approx 0.5 \mu\text{m}$ ) and is certainly smaller than the pitch length of the helical structure  $d$ : typically,  $d \approx 10$  and  $50 \mu\text{m}$  for the exo- and endocuticles, respectively. A typical value

of  $G_h$  may be approximately  $1 \text{ J m}^{-2}$ , which leads to the estimation  $G \approx 500\text{--}1000 \text{ J m}^{-2}$ .

Equation (12) predicts that the helical composite is reinforced compared with the parallel structure in any direction: the toughness of the helical structure is larger than the toughness of the parallel structure in the toughest direction,  $G_h$ . Note here that  $G_h$  appears in Equation (12) instead of  $G_s$  because, for a crack tip in a soft layer to advance, the tip has to break the next hard layer.

From Equations (12) and (13), we can draw a number of guiding principles for toughening materials with helical structures. For example, to enlarge the factor  $d/a_0$ , it is advantageous to use thinner bundles forming a helical structure with a larger pitch; to make the factor  $e'$  smaller, it is advantageous that the matrix is hard and the bundles are soft, and that the volume fraction of the hard and soft elements is of the same order ( $(e')^{-1}$  has a sharp peak as a function of  $\delta$ ). These principles, the helical pitch larger than bundle thickness, the combination of soft bundles and a hard matrix and an equal volume fraction of the soft and hard elements, are indeed used in the exoskeleton of crustaceans as already described.

Equation (12) also explains another clever feature of the crustacean: in the exoskeleton, the exocuticle with a small helical pitch covers the endocuticle with a large helical pitch. This feature is significantly advantageous in a mechanical sense, as understood from Equation (12). This expression is valid for a crack of size  $a$  that is larger than  $d$ . In this case, however, a helical structure with a long pitch  $d$  cannot be



**Figure 6** Double protection by the exocuticle with a small helical pitch and the endocuticle with a large helical pitch. The exocuticle protects the inside for small cracks with a small toughness, whereas the endocuticle protects the inside for large cracks with a large toughness.

protected for small cracks. In the exoskeleton, as illustrated in Figure 6, the exocuticle protects the inside from smaller cracks with smaller toughness, whereas the endocuticle protects the inside from larger cracks with larger toughness; note that the stress concentration is significant for larger cracks.

Overall, the helical structure composed of thin fibers is a very smart structure. Bundles or fibers are generally extremely tough in the longitudinal direction but extremely weak in the transverse direction. For example, the toughness of glass fibers increases in the longitudinal direction when the radius decreases. Then, bundles oriented parallel throughout a matrix would be a smart structure for the longitudinal direction. However, as shown in the simple theory, by forming a helical composite structure with a matrix, the helical composite becomes tougher than the parallel composite even in the toughest direction of the parallel composite.

### SPIDER WEBS

Spider silks have been actively studied as a high-performance polymeric fiber, which leads to various reasons for their mechanical superiority, such as entropic elasticity,<sup>58</sup> water coating,<sup>59</sup> breaking strength,<sup>60</sup> gene family,<sup>61</sup> liquid-crystalline structures,<sup>62</sup> micellar structures,<sup>63,64</sup> and hierarchical structures,<sup>65</sup> and torsional relaxation.<sup>66</sup> Spider webs seem to be a highly optimized lightweight structure,<sup>67</sup> likely as a result of their evolution from the Jurassic period or earlier.<sup>68</sup> However, the mechanical advantages of the spider orb webs have been less studied: only their structural vibration,<sup>69,70</sup> tensile pre-stress,<sup>71</sup> detailed finite-element modeling<sup>70,72</sup> and nonlinear response<sup>73–75</sup> have been studied.

Here, we focus on orb webs among other web varieties<sup>76</sup> and construct a simple model of spider webs,<sup>77</sup> to show the physical principles of the mechanical advantages. The simple model of spider webs is composed of radial and spiral threads, as in Figure 7. The model is under a global strain of 0.1, as in real webs.<sup>72</sup> Under pre-tension, the force distribution is not homogeneous, and the maximum force acts on the radial springs at the edges, as indicated in Figure 7.

One of the aims of this study is to investigate the importance of the combination of hard and soft elements. Orb spider webs are composed of spiral and radial threads, in which the spiral threads are thinner and softer than the radial threads.

To this end, we examined the maximum force at the edge radial springs in the web under pre-tension. A web with a small maximum

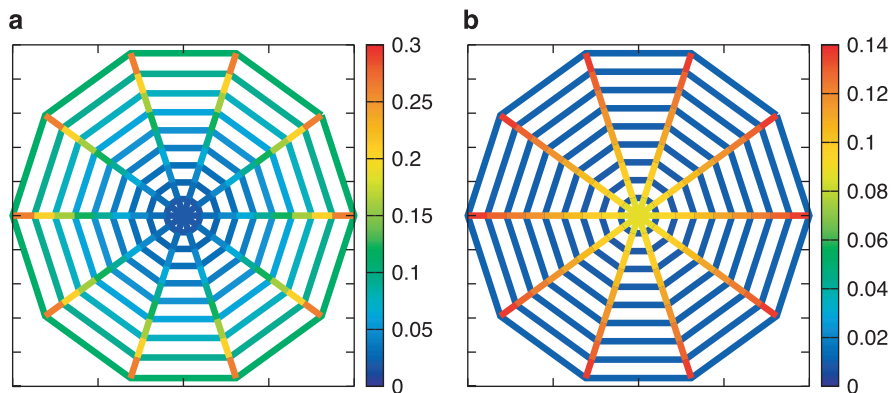


**Figure 7** Force distribution in the simple model of spider webs under tension. The spring constant of spiral threads per unit length is the same as that of radial threads in the left, whereas the former is smaller than the latter in the right ( $K/k$  is 1 in the left and 10 in the right). Reprinted from Aoyanagi and Okumura<sup>77</sup> © 2013, American Physical Society.



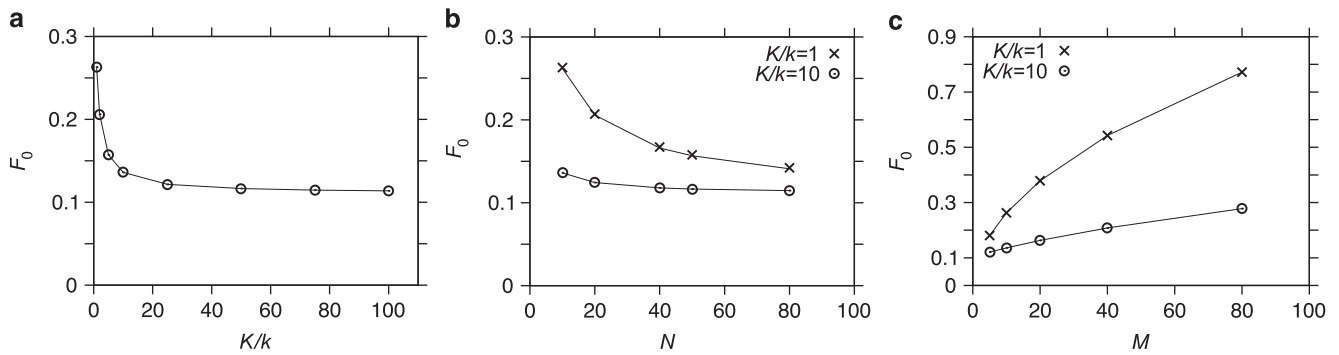


**Figure 8** Maximum force that appears in the web as a function of the spring constant (per unit length) of the radial threads over that of the spiral threads  $K/k$  (left), as a function of the number of radial threads  $N$  (middle) and the number of spiral threads  $M$  (right). Reprinted from Aoyanagi and Okumura<sup>77</sup> © 2013, American Physical Society.

force is considered to be strong because materials generally begin failing at the position where a strong local force acts.

As demonstrated in Figure 7, the web is stronger, that is, the maximum force is smaller, when the stiffness contrast is larger. The (normalized) maximum force at the edges is 0.3 in the left and 0.14 in the right.

Surprisingly, the stiffness difference appears to be optimized in real webs because of at least three mechanical factors, providing high adaptability to spiders. One factor is revealed in the left plot in Figure 8, in which the maximum force at the edges (a measure of the weakness of the web) is shown as a function of the stiffness difference  $K/k$ . The maximum force sharply decreases in a range of small  $K/k$  but changes only slightly when  $K/k$  is larger than approximately 14, which is a typical value of the stiffness difference in real webs.<sup>72</sup> Considering the difficulty for spiders to create two types of threads whose mechanical properties are quite different, the typical value of the stiffness difference (14) may be regarded as a result of optimization. Other mechanical advantages of the large stiffness difference are demonstrated in the middle and right plots in Figure 8, in which the strength of the web is less susceptible to changes in the number of either spiral or radial threads when  $K/k$  is larger. These properties allow high flexibility for survival of spiders: spiders can span webs by freely selecting the numbers of spiral and radial threads, according to the spacial and biological environments, for example, to a typical tree branch spacing or to a typical prey size.

In addition, it was shown that no stress concentration occurs in the simple model of the web. Even if a part of a spiral thread is removed from the model web, the forces acting on the parts of spiral threads near the missing part are not enhanced in a new equilibrium state. This result explains that spider webs function well even if some parts of spiral threads are missing, which illustrates the robustness of spider webs.

## DISCUSSION

We have demonstrated several examples of biocomposites reinforced by structures, in particular, by the fusion of soft and hard elements. In the case of nacre, in addition to the soft–hard combination, the hierarchical structure is important for the reinforcement. A number of scaling laws predicted from the theory were found to be robust. Although the scaling laws are generally expected to be valid only in limiting cases, these scaling laws can be valid in a wide practical range. The model of nacre could also aid in understanding the sophisticated structure found in the cuticles of crustaceans. We have also explored mechanical advantages of the combination of the soft and hard threads in spider webs. The scaling laws collectively presented in this review,

together with physical understandings and guiding principles for smart design based on simple models, may inspire researchers to create tough materials and to construct more elaborate models. In this respect, some other simple ideas for nonlinear and porous materials that have also been discussed, for example, in Nakagawa and Okumura,<sup>78</sup> Aoyanagi and Okumura,<sup>79</sup> Soné *et al.*<sup>80</sup>; Kashima and Okumura<sup>81</sup> may also be useful.

In this review, we have observed that simple linear models can explain the essential physics in many cases. However, nonlinear treatments could be essential in some cases. We envision that the nonlinear extension will have an important role in the future study of biomaterials based on simple scaling arguments.

## ACKNOWLEDGEMENTS

This research was partly supported by the Grant-in-Aid for Scientific Research on Innovative Areas, ‘Fusion Materials (area no. 2206),’ of MEXT, Japan, and by the Grant-in-Aid for Scientific Research (A) (no. 24244066) of JSPS, Japan.

- Meyers, M. A., Lin, A. Y., Seki, Y., Chen, P.-Y., Kad, B. K., Bodde, S. Structural biological composites: an overview. *JOM* **58**, 35–41 (2006).
- Fratzl, P., Weinkamer, R. Nature's hierarchical materials. *Prog. Mater. Sci.* **52**, 1263–1334 (2007).
- Ji, B., Gao, H. Mechanical principles of biological nanocomposites. *Ann. Rev. Mater. Res.* **40**, 77–100 (2010).
- Vincent, J. *Structural Biomaterials* (Princeton University Press, Princeton, New Jersey, 2012).
- Sumitomo, T., Kakisawa, H., Owaki, Y., Kagawa, Y. *In situ* transmission electron microscopy observation of reversible deformation in nacre organic matrix. *J. Mater. Res.* **23**, 1466–1471 (2008).
- Jackson, A., Vincent, J., Turner, R. The mechanical design of nacre. *Proc. Royal Soc. (London) B* **234**, 415 (1988).
- Sachs, C., Fabritius, H., Raabe, D. Hardness and elastic properties of dehydrated cuticle from the lobster *homarus americanus* obtained by nanoindentation. *J. Mater. Res.* **21**, 1987–1995 (2006).
- Emler, R. Echinoderm calcite: a mechanical analysis from larval spicules. *Biol. Bull.* **163**, 264–275 (1982).
- Aizenberg, J., Weaver, J., Thanawala, M., Sundar, V., Morse, D., Fratzl, P. Skeleton of *Euplectella* sp.: structural hierarchy from the nanoscale to the macroscale. *Science* **309**, 275–278 (2005).
- Hamm, C. E., Merkel, R., Springer, O., Jurkojc, P., Maier, C., Prechtel, K., Smetacek, V. Architecture and material properties of diatom shells provide effective mechanical protection. *Nature* **421**, 841–843 (2003).
- Sarikaya, M., Liu, J., Aksay, I. *Biomimetics: Design and Processing of Materials* 35–90 (AIP, New York, 1995).
- Kamat, S., Su, X., Ballarini, R., Heuer, A. Structural basis for the fracture toughness of the shell of the conch *strombus gigas*. *Nature* **405**, 1036–1040 (2000).
- Gao, H., Ji, B., Jäger, I., Arzt, E., Fratzl, P. Materials become insensitive to flaws at nanoscale: lessons from nature. *Proc. Natl Acad. Sci. USA* **100**, 5597 (2003).
- Mayer, G. Rigid biological systems as models for synthetic composites. *Science* **310**, 1144 (2005).

- 15 Currey, J. D. *Bones: Structure and Mechanics* (Princeton University Press, Princeton, New Jersey, 2002).
- 16 Fratzl, P., Gupta, H., Paschalis, E., Roschger, P. Structure and mechanical quality of the collagen-mineral nano-composite in bone. *J. Mater. Chem.* **14**, 2115–2123 (2004).
- 17 Hellmich, C., Barthélémy, J.-F., Dormieux, L. Mineral-collagen interactions in elasticity of bone ultrastructure—a continuum micromechanics approach. *Eur. J. Mech. A* **23**, 783–810 (2004).
- 18 Kato, T. Polymer/calcium carbonate layered thin-film composites. *Adv. Mater.* **12**, 1543–1546 (2000).
- 19 Sarikaya, M., Tamerler, C., Jen, A., Schulten, K., Baneyx, F. Molecular biomimetics: nanotechnology through biology. *Nat. Mater.* **2**, 577–585 (2003).
- 20 Deville, S., Saiz, E., Nalla, R., Tomsia, A. Freezing as a path to build complex composites. *Science* **311**, 515–518 (2006).
- 21 Munch, E., Launey, M., Alsem, D., Saiz, E., Tomsia, A., Ritchie, R. Tough, bio-inspired hybrid materials. *Science* **322**, 1516 (2008).
- 22 Bonderer, L., Studart, A., Gauckler, L. Bioinspired design and assembly of platelet reinforced polymer films. *Science* **319**, 1069 (2008).
- 23 Corte, L., Leibler, L. A model for toughening of semicrystalline polymers. *Macromolecules* **40**, 5606–5611 (2007).
- 24 Li, X., Chang, W., Chao, Y., Wang, R., Chang, M. Nanoscale structural and mechanical characterization of a natural nanocomposite material: the shell of red abalone. *Nano Lett.* **4**, 613–617 (2004).
- 25 Barthelat, F., Li, C., Comi, C., Espinosa, H. Mechanical properties of nacre constituents and their impact on mechanical performance. *J. Mater. Res.* **21**, 1977–1986 (2006).
- 26 Barthelat, F., Tang, H., Zavattieri, P., Li, C., Espinosa, H. On the mechanics of mother-of-pearl: a key feature in the material hierarchical structure. *J. Mech. Phys. Solids* **55**, 306–337 (2007).
- 27 Meyers, M., Lin, A., Chen, P., Muyco, J. Mechanical strength of abalone nacre: role of the soft organic layer. *J. Mech. Behav. Biomed. Mater.* **1**, 76–85 (2008).
- 28 Okumura, K., de Gennes, P.-G. Why is nacre strong? Elastic theory and fracture mechanics for biocomposites with stratified structures. *Eur. Phys. J. E* **4**, 121–127 (2001).
- 29 Smith, B., Schäffer, T., Viani, M., Thompson, J., Frederick, N., Kindt, J., Belcher, A., Stucky, G., Morse, D., Hansma, P. Molecular mechanistic origin of the toughness of natural adhesives, fibres and composites. *Nature* **399**, 761–763 (1999).
- 30 Rao, M. P., Sanchez-Herencia, A., Beltz, G., McMeeking, R., Lange, F. Lamellar ceramics that exhibit a threshold strength. *Science* **286**, 102–105 (1999).
- 31 Evans, A., Suo, Z., Wang, R., Aksay, I., He, M., Hutchinson, J. Model for the robust mechanical behavior of nacre. *J. Mater. Res.* **16**, 2476 (2001).
- 32 Song, F., Soh, A., Bai, Y. Structural and mechanical properties of the organic matrix layers of nacre. *Biomaterials* **24**, 3623–3631 (2003).
- 33 Okumura, K. Why is nacre strong? ii. Remaining mechanical weakness for cracks propagating along the sheets. *Eur. Phys. J. E* **7**, 303–310 (2002).
- 34 de Gennes, P.-G., Okumura, K. On the toughness of biocomposites. *Comp. Ren. Acad. Sci. IV* **1**, 257–261 (2000).
- 35 Okumura, K. Fracture strength of biomimetic composites: scaling views on nacre. *J. Phys.: Cond. Matt.* **17**, S2879 (2005).
- 36 Okumura, K. Enhanced energy of parallel fractures in nacre-like composite materials. *Europhys. Lett.* **63**, 701 (2003).
- 37 Kotha, S., Li, Y., Guzelsu, N. Micromechanical model of nacre tested in tension. *J. Mater. Sci.* **36**, 2001–2007 (2001).
- 38 Katti, D., Katti, K., Sopp, J., Sarikaya, M. 3d finite element modeling of mechanical response in nacre-based hybrid nanocomposites. *Comp. Theor. Polym. Sci* **11**, 397–404 (2001).
- 39 Ji, B., Gao, H. Mechanical properties of nanostructure of biological materials. *J. Mech. Phys. Solid* **52**, 1963–1990 (2004).
- 40 Nukala, P., Zapperi, S., Šimunović, S. Statistical properties of fracture in a random spring model. *Phys. Rev. E* **71**, 066106 (2005).
- 41 Fratzl, P., Gupta, H., Fischer, F., Kolednik, O. Hindered crack propagation in materials with periodically varying young's modulus from biological materials. *Adv. Mater.* **19**, 2657–2661 (2007).
- 42 Hamamoto, Y., Okumura, K. Analytical solution to a fracture problem in a tough layered structure. *Phys. Rev. E* **78**, 026118 (2008).
- 43 Hamamoto, Y., Okumura, K. Realistic numerical analysis of a bioinspired layered composite with a crack: robust scaling laws and crack arrest. *Adv. Eng. Mater.* **15**, 522–528 (2013).
- 44 Aoyanagi, Y., Okumura, K. Stress and displacement around a crack in layered network systems mimicking nacre. *Phys. Rev. E* **79**, 066108 (2009).
- 45 Beyerlein, I. J., Phoenix, S. L., Sastry, A. M. Comparison of shear-lag theory and continuum fracture mechanics for modeling fiber and matrix stresses in an elastic crack composite lamina. *Int. J. Solid. Struct.* **33**, 2543–2574 (1996).
- 46 Weaver, J., Milliron, G., Miserez, A., Evans-Lutterodt, K., Herrera, S., Gallana, I., Mershon, W., Swanson, B., Zavattieri, P., DiMasi, E., Kisailus, D. The stomatopod dactyl club: a formidable damage-tolerant biological hammer. *Science* **336**, 1275–1280 (2012).
- 47 Nikolov, S., Petrov, M., Lymperakis, L., Friák, M., Sachs, C., Fabritius, H., Raabe, D., Neugebauer, J. Revealing the design principles of high-performance biological composites using ab initio and multiscale simulations: the example of lobster cuticle. *Adv. Mater.* **22**, 519–526 (2010).
- 48 Fabritius, H., Sachs, C., Triguero, P., Raabe, D. Influence of structural principles on the mechanics of a biological fiber-based composite material with hierarchical organization: the exoskeleton of the lobster homarus americanus. *Adv. Mater.* **21**, 391–400 (2009).
- 49 Kato, T., Sugawara, A., Hosoda, N. Calcium carbonate-organic hybrid materials. *Adv. Mater.* **14**, 869–877 (2002).
- 50 Yamamoto, Y., Nishimura, T., Sugawara, A., Inoue, H., Nagasawa, H., Kato, T. Effects of peptides on caco3 crystallization: mineralization properties of an acidic peptide isolated from exoskeleton of crayfish and its derivatives. *Cryst. Growth Des.* **8**, 4062–4065 (2008).
- 51 Sugawara, A., Nishimura, T., Yamamoto, Y., Inoue, H., Nagasawa, H., Kato, T. Self-organization of oriented calcium carbonate/polymer composites: effects of a matrix peptide isolated from the exoskeleton of a crayfish. *Angew. Chem. Int. Ed.* **45**, 2876–2879 (2006).
- 52 Okumura, K. Simple model for the toughness of a helical structure inspired by the exoskeleton of lobsters. *J. Phys. Soc. Jpn* **82**, 124802 (2013).
- 53 Hull, D., Clyne, T. *An Introduction to Composite Materials* (Cambridge University Press, Cambridge, 1996).
- 54 Gao, H. Fracture analysis of nonhomogeneous materials via a moduli-perturbation approach. *Int. J. Solid. Struct.* **27**, 1663–1682 (1991).
- 55 Muju, S. Crack propagation in bimaterial multilayered periodically microcracking composite media. *Compos. Sci. Technol.* **60**, 2213–2221 (2000).
- 56 Fischer, F., Predan, J., Fratzl, P., Kolednik, O. Semi-analytical approaches to assess the crack driving force in periodically heterogeneous elastic materials. *Int. J. Fract.* **173**, 57–70 (2012).
- 57 Kolednik, O., Predan, J., Fischer, F., Fratzl, P. Bioinspired design criteria for damage-resistant materials with periodically varying microstructure. *Adv. Funct. Mater.* **21**, 3634–3641 (2011).
- 58 Gosline, J. M., Denny, M. W., DeMont, M. E. Spider silk as rubber. *Nature* **309**, 551–552 (1984).
- 59 Vollrath, F., Edmonds, D. T. Modulation of the mechanical properties of spider silk by coating with water. *Nature* **340**, 305–307 (1989).
- 60 Osaki, S. Spider silk as mechanical lifeline. *Nature* **384**, 419–419 (1996).
- 61 Guerette, P. A., Ginzinger, D. G., Weber, B. H., Gosline, J. M. Silk properties determined by gland-specific expression of a spider fibroin gene family. *Science* **272**, 112–115 (1996).
- 62 Vollrath, F., Knight, D. P. Liquid crystalline spinning of spider silk. *Nature* **410**, 541–548 (2001).
- 63 Jin, H.-J., Kaplan, D. L. Mechanism of silk processing in insects and spiders. *Nature* **424**, 1057–1061 (2003).
- 64 Emile, O., Le Floch, A., Vollrath, F. Biopolymers: shape memory in spider draglines. *Nature* **440**, 621–621 (2006).
- 65 Zhou, H., Zhang, Y. Hierarchical chain model of spider capture silk elasticity. *Phys. Rev. Lett.* **94**, 028104 (2005).
- 66 Emile, O., Le Floch, A., Vollrath, F. Time-resolved torsional relaxation of spider draglines by an optical technique. *Phys. Rev. Lett.* **98**, 167402 (2007).
- 67 Witt, P. N., Reed, C. F. Spider-web building. *Science* **149**, 1190–1197 (1965).
- 68 Selden, P. Orb-web weaving spiders in the early cretaceous. *Nature* **340**, 711–713 (1989).
- 69 Masters, W. M. Vibrations in the orbwebs of nuctenea sclopetaria (araneidae). *Behav. Ecol. Sociobiol.* **15**, 207–215 (1984).
- 70 Lin, L., Edmonds, D., Vollrath, F. Structural engineering of an orb-spider's web. *Nature* **373**, 146–148 (1995).
- 71 Wirth, E., Barth, F. G. Forces in the spider orb web. *J. Comp. Physiol. A* **171**, 359–371 (1992).
- 72 Alam, M., Wahab, M., Jenkins, C. Mechanics in naturally compliant structures. *Mech. Mater.* **39**, 145–160 (2007).
- 73 Cranford, S., Tarakanova, A., Pugno, N., Buehler, M. Nonlinear material behaviour of spider silk yields robust webs. *Nature* **482**, 72–76 (2012).
- 74 Ackbarow, T., Sen, D., Thaulow, C., Buehler, M. J. Alpha-helical protein networks are self-protective and flaw-tolerant. *PLoS ONE* **4**, e6015 (2009).
- 75 Buehler, M. J., Ackbarow, T. Fracture mechanics of protein materials. *Mater. Today* **10**, 46–58 (2007).
- 76 Vollrath, F., Selden, P. The role of behavior in the evolution of spiders, silks, and webs. *Ann. Rev. Ecol. Evol. Systematics* **38**, 819 (2007).
- 77 Aoyanagi, Y., Okumura, K. Simple model for the mechanics of spider webs. *Phys. Rev. Lett.* **104**, 038102 (2010).
- 78 Nakagawa, S., Okumura, K. Crack-tip stress concentration and mesh size in networks. *J. Phys. Soc. Jpn* **76**, 4801 (2007).
- 79 Aoyanagi, Y., Okumura, K. Crack-tip stress concentration and structure size in nonlinear structured materials. *J. Phys. Soc. Jpn* **78**, 034402 (2009).
- 80 Soné, N., Mori, M., Okumura, K. Scaling relation in fracture of the materials with elastoplastic response inaccessible by scaling laws. *J. Phys. Soc. Jpn* **81**, 074604 (2012).
- 81 Kashiwaga, Y., Okumura, K. Fracture of soft foam solids: interplay of visco-and plasto-elasticity. *ACS Macro Lett.* **3**, 419–422 (2014).